Design of M3FCM based Convolutional Neural Network for Prediction of Wheat Disease

Dr. V. Gokula Krishnan[*1], Dr. M. V. Vijaya Saradhi[2], G. Dhanalakshmi[3], C. S. Somu[4], Dr. W. Gracy Theresa[5]

Abstract*:* Wheat is the primary source of nutrition for more than two-thirds of the world's population. Wheat can be adversely affected by a number of diseases, resulting in lower yields and, in severe cases, famine. Plants are negatively impacted by illnesses in leaves, a type of sickness. Rapid and precise recognition methods must be used in practice in order to minimize losses. This research study focuses on the segmentation of afflicted regions in order to diagnose the plant disease rapidly and enhance crop quality, therefore solving this problem. As a result, the existing fuzzy c-means clustering (FCM) procedure is highly sensitive to noise, and local spatial information is frequently introduced, resulting in a high computational complexity, which arises from an iterative calculation of the distance between pixels in local spatial neighbors and clustering centers. This study proposes a faster and more reliable FCM technique called marker and mask based membership filtering (M3FCM) to overcome this problem. As a first step, morphological reconstruction is used to incorporate images' local spatial information into M3FCM, ensuring noise protection and image part preservation. Second, local membership filtering relies solely on the spatial neighbors of the membership partition to replace the modification of membership divider based on the distance among pixels inside local spatial neighbors and clustering centers. Kaggle images serve as training and testing for the CNN classification system. The suggested segmentation model achieved 98.06 percent accuracy, while the CNN model scored 94.91 percent accuracy in the experiment.

Keywords: *Classification, Convolutional Neural Network, Fuzzy C-Means Clustering (FCM), Prediction, Segmentation, Wheat Disease.*

1. Introduction

Wheat is a major crop and a major source of sustenance for humans around the world [1]. Wheat is the most widely planted crop in the world, and its output is critical to the well-being of most countries' populations. One of the most significant determinants in wheat yield is fungal diseases, such as rust, septoria, and powdery mildew [2]. In addition to leaf rust, powdery mildew, and septoria (infections such as Puccinia triticina, there are a number of other pathogens that can be found all over the world. These pathogens can be found on a wide range of grain crops as part of the phytopathogenic complex. Fungicides, however, can limit the damage caused by causative agents of the above-mentioned diseases to a maximum of 20% [3]. The economic impact of yellow and stem rust epiphytes, which have led to grain shortages of more than 30%, is significant. Grain yield losses from various diseases can range anywhere from 15% to 30% or more [4, 5], depending on the

1Professor, Department of CSE, Saveetha School of Engineering, Saveetha Institute of Medical and Technical Sciences, Thandalam, Chennai, Tamil Nadu, India.
ORCID ID : 0000-0002-3913-3156
2 Professor & Head, Department of CSE, ACE Engineering College, Ghatkesar, Hyderabad, Telangana, India.
3 Associate Professor, Department of IT, Panimalar Engineering College, Poonamallee, Chennai, Tamil Nadu, India.
4 Assistant Professor, Department of CSE, Rajalakshmi Institute of Technology, Chennai, Tamil Nadu, India.
5 Associate Professor, Department of CSE, Panimalar Engineering College, Poonamallee, Chennai, Tamil Nadu, India.
* Corresponding Author Email: gokul_kris143@yahoo.com

region and season.

Preventing and responding to these diseases is the most effective strategy to combat them [6, 7]. Such a method, however, is unachievable unless diseases are diagnosed quickly and correctly. In this instance, it is critical to diagnose infections during the seedling stage, as resistance to the pathogen is increased at later stages of plant development [8]. A correct diagnosis is only as good as the amount of time, effort, and resources it takes to perform it. All through wheat agriculture, the primary method of disease diagnosis has been visual inspection. Plaque, pustules, spots, and necrosis can all be identified using this method [9, 10]. Additionally, it demands a great deal of training in phytopathology and a lot of tedious effort (keeping a record book, statistical processing of observations, etc.). A number of new techniques have been developed in the last few decades, such as molecular, spectral, and digital picture analysis [11- 12]. Each of these methods has a different level of effort, cost, and precision. Colour, texture, and shape changes in plant organs can be determined using digital RGB photographs, which are analysed for changes in pigment composition under the effect of pathogen activity [13–17]. Using a digital camera or cell phone is all that is needed to monitor an area, making it a low-cost and fast technique. There are some drawbacks, such as reduced sensitivity (in comparison, for example, with spectral approaches [18]).

Machine learning approaches based on neural network algorithms have recently given a major boost to plant-disease monitoring technology based on digital RGB photos. Multiple plant diseases were successfully detected using deep learning neural networks. Researchers have shown that machine learning techniques like support vector machines, random forests, and stochastic gradient

descent can be outperformed by deep learning approaches. For better disease recognition in plants, deep learning methods have included transfer learning approaches, networks with varied designs, working with limited data and Bayesian deep learning. Compared to other methods, deep learning neural networks include a layered architecture of neurons, in which the output of the preceding layer is used as input data to derive concepts about the investigated objects [19, 20]. Convolutional neural networks (CNNs), which come in a variety of design options, are among the most successful methods for such a critical task as picture labelling. AlexNet [21] and VGG [22] were two of the early CNN architectures. [23-25] of responses across channels (SENet network) through further development of these approaches. These developments have made deep learning neural networks more widely applicable. In addition, they've had outstanding success with more difficult plant phenotyping issues [26–30].

For image segmentation, we've developed a substantially faster and more robust approach. With a low computing cost and excellent segmentation precision, the proposed technique can successfully segment a wide range of images. The following is a list of the most significant contributions.

To increase noise-immunity and picture detail-preservation simultaneously, the proposed M3FCM leverages morphological reconstruction (MR) to smooth images. This eliminates the need to select separate filters for different types of noise in existing improved FCM algorithms. Because of this, the M3FCM method is superior to the others when dealing with noise-corrupted images.

A low computational cost is achieved by applying a quick membership filtering instead of a slower distance computation among pixels inside local spatial neighbours and their clustering centres in the proposed M3FCM method. M3FCM is therefore more efficient than previous FCM algorithms.

What follows is a breakdown of the rest of the document: In Section II, we present a list of previous studies on the detection of plant diseases. Our model and algorithm are outlined in Section III. Section IV explains the outcomes of experiments on publicly available datasets. Section V, our final section, presents our findings and recommendations.

2. Related Works

A new wheat disease categorization approach has been proposed by Goyal, L. [31]. A novel deep learning model has been taught to effectively identify wheat illnesses into ten different categories. The proposed testing procedure has a 97.88 percent success rate. The accuracy metric is also improved by 7.01 percent and 15.92 percent when compared to VGG16 and RESNET50, the two most popular deep learning models. Experiments show that other parameters such as precision, recall, and f-score are improved by the proposed strategy.

Early detection models utilizing machine learning with hyper spectral images have been presented by Khan IH [32]. Prior to comparing powdery mildew and healthy wheat, this study used NDTIs and VIs to better distinguish between the two varieties. In order to identify powdery mildew, linear discrimination examination was used to aggregate the most optimal features (i.e., VIs & NDTIs). In addition, researchers devised a regression model based on the partial least squares regression to determine the severity of the condition (DS). An overall accuracy of 82.35% and a Kappa coefficient of 0.56 were achieved by applying the discriminant model with the combined VIs & NDTIs to identify the diseased leaves, with inconspicuous symptoms that were

difficult to detect as symptoms of disease using the previous method. It was also found that the calibrated and validated DSM estimate model performed well, with an R2 coefficient in the range of 0.748% and 0.722%, respectively. As a result, this detection method, as well as the quantification perfect, appears promise for the early detection of illness in crops

Using spectroscopy, A. Wójtowicz (Ph.D., University of Warsaw) [33] attempted to identify and distinguish at the leaf scale the leaf rust symptoms induced by two closely connected special forms of Puccinia spp. We used a FieldSpec 3 spectrometer to take data in the 350–2500 nm range. For each of the Random Forest models, a pure spectra test was performed to determine the vegetation index. Uredinia could be distinguished from other symptoms on rye and wheat leaves by using three vegetative indices: CRI, PRI, and GNDVI. The model based on the specified spectral wavelengths had a higher hit rate (96.6%) than forecasts based solely on vegetative indices, as the results of the analysis revealed (Hit Rate of 91.7 percent). Both methods demonstrate the usefulness of high-quality spectrum goods like satellite photos in reducing crop protection operational expenses.

Schirrmann, M., [34] used a deep residual neural network to detect Stripe rust (Pst) signs in winter wheat canopies (ResNet). A conventional RGB camera installed on a platform at a height of 2 m was used to compile a big database of annotations for this purpose. Moving over a Pst-inoculated and Pst-free field trial, the platform captured images of winter wheat plants. In order to train the image classifier, we used the original, unprocessed camera photos to create 224 x 224 px patches. Various stages of the illness outbreak were used to train the image classifier. The picture classifier's overall accuracy was 90 percent at patch level. 224 px stride length was used to evaluate the image classifier at the picture level. This allowed for quick test performance. Image classifier achieved a 77 percent accuracy rate at the image level. An accuracy of 57% was achieved even at the earliest stages of Pst's outbreak, when the disease was only expanding at a rate of 0.5%. Detection accuracy of 76% was achieved while the Pst outbreak was still in its early stages, with only 2–4% of cases reported.

T. Hayit [35] suggests using computerized models to identify the strain of yellow rust disease that has infected a particular wheat crop. The Yellow-Rust-Xception model, based on deep convolutional neural networks, was presented here. Rust-infected wheat leaf images are fed into a computer model that classifies them into one of five categories. Yellow-Rust-Xception was tested with a 91% accuracy rate using a fresh dataset of wheat leaf photos infected with yellow rust. Wheat yellow rust severity can be assessed with Yellow Rust-Xception.

There are five fungal diseases of wheat shoots that have been identified by Genaev, M.A. [36], and this method can be used to identify the stage of plant growth for each of the five diseases (leaf rust, stem rust, yellow rust). 2414 photos depicting different wheat fungus disease types were created and then expertly labeled according to disease type (WFD2020). There are more than 80 percent single disease labels (including seedlings) in the dataset, more than 12 percent healthy plants, and 6 percent photos labeled with multiple diseases. Using an image hashing algorithm, a technique for reducing training data degeneracy was used to create this collection. On the basis of the EfficientNet architecture, the disease-recognition algorithm is built. On average, an image style transfer and enhancement training technique yielded an accuracy of 0.942%.

3. Proposed System

3.1. Dataset Description

Researchers studying plant disease detection using computer vision could benefit from this dataset. Healthy, Stripe Rust and Septoria wheat leaf picture were employed in this work for experimenting. 102 healthy, 208 stripe rust, and 97 septoria-detected wheat leaves were found in the data set. Pictures from https://www.kaggle.com/datasets/olyadgetch/wheat-leaf-dataset are used in this post. 80 percent of the photos were utilized for training, l0 percent for validation, and the remaining 10 percent were used for testing. Holeta wheat farm, Ethiopia, is where the data was collected, and it was taken in an uncontrolled environment Canon EOS 5D Mark III, was used to capture this image. Figure 1 displays a selection of the dataset's photos.

Fig. 1. Sample images of wheat.

3.2. Preprocessing

Three models, such as the Star Shape Search pattern (SSSP), the Laplacian-of-Gaussian (LoG), and histogram equalization, are combined in this novel hybrid model. The undesired distortions are initially divided into two blocks, the first of which is processed using the SSSP and the second of which is handled using the LoG pattern. The categorization accuracy is much enhanced by combining these two strategies. Using the histogram equalization approach, the final step in improving image contrast is completed.

3.2.1. Working of Star Shape Search pattern
This Search pattern does not function for the entire 2-D image, but rather only works for those areas where the noisy pixels have been recognized. The de-noisy pixel computation formula is given in equation 1 below.

$$De - noise\ pixel = sum\ (sssp1)\ /\ length\ (sssp1) \qquad (1)$$

3.2.2. Laplacian of Gaussian (LoG)

Derivative filters such as Laplacian filters can be used to identify regions in photographs where there is fast change (or "edges"). Prior to using the Laplacian filter, it is usual practise to lessen the sum of noise extant in the image using a Gaussian filter. The Laplacian of Gaussian (LoG) operation is a two-step technique.

$$L(x,y) = \nabla^2 f(x,y) = \frac{\partial^2 f(x,y)}{\partial x^2} + \frac{\partial^2 f(x,y)}{\partial y^2} \qquad (2)$$

In order to approximate the Laplacian effect, one can find an approximation discrete convolution kernel in a variety of ways. As an example, suppose that

$$\begin{bmatrix} 0 & 1 & 0 \\ 1 & -4 & 1 \\ 0 & 1 & 0 \end{bmatrix} \qquad (3)$$

A Laplacian with a negative central peak is called a negative Laplacian. To obtain a positive Laplacian, use -1s and a +4 to reverse the signs of the elements. This is irrelevant. Combining the Laplacian and Gaussian functions into a single equation will yield a smoothing Gaussian filter:

$$LoG(x,y) = -\frac{1}{\pi\sigma^2}\left[1 - \frac{x^2+y^2}{2\sigma^2}\right]e^{-\frac{x^2+y^2}{2\sigma^2}} \qquad (4)$$

Using the LoG operator, one can compute the image's second derivative. The LoG will return zero if the image is essentially uniform. The LoG will respond positively to changes on the darker side, and negatively to changes on the brighter side, depending on the nature of the alteration.

3.2.3. Luminance adaptive contrast improvement

To recover the contrast of the noise-free image R', we use an effective haze reduction method.

$$R' = t.J + (1 - t).A \qquad (5)$$

For example, if A is a measure of global illumination. Without any foggy depravation, J represents the original item or scene's intensity. t is the percentage of light emitted from the scene or object that reaches the camera. t is calculated based on the available data.

$$t(x) = 1 - \omega.\min_{c\epsilon\{r,g,b\}}\left(\min_{y\epsilon\Omega(x)}\left(\frac{R'c(y)}{A^c}\right)\right) \qquad (6)$$

In this study, the block size is 3 x 3 and x is a local block centered at pixel x.

3.3. Segmentation

We use MR instead of mean or median filters in this investigation because of its ability to withstand noise. MR is capable of effectively suppressing a wide range of noise, regardless of its type. Furthermore, for the implementation of the MR algorithm, making it faster. An image that was reconstructed by MR is used to perform clustering on the grey level histogram of the picture to produce the fuzzy matrix via iteration. [37] In the final step, a filter is used to alter the membership partition matrix. We can get a satisfactory segmentation result in a shorter amount of time using this strategy.

3.3.1. General Impression of the Proposed Methodology

Clustering on the grey level histogram is used in the proposed M3FCM like in EnFCM, and the goal function can be stated as

$$J_m = \sum_{l=1}^{q}\sum_{k=1}^{c}\gamma l u_{kl}^m||\xi_l - v_k||^2 \qquad (7)$$

Where u_{kl} represents cluster k's fuzzy membership in the grey value l

$$\sum_{l=1}^{q}\gamma l = N \qquad (8)$$

Where ξ is an image reconstructed by MR, and ξ_l is a gray level, $1 \le l \le q$, q represents the number of grey levels in, which is typically significantly smaller than N.

$$\xi = R^c(f) \qquad (9)$$

Where $R^\wedge C \ f$ stands for an original picture, while denotes morphological closing reconstruction.

An optimization problem can be transformed into an unconstrained optimization problem that minimizes the following objective function using the Lagrange multiplier technique:

$$J_m = \sum_{l=1}^{q} \sum_{k=1}^{c} \gamma l u_{kl}^{m} ||\xi_l - v_k||^2 - \lambda(\sum_{k=1}^{c} u_{kl} - 1) \qquad (10)$$

Where λ is a multiplier by Lagrange. A Lagrange function with an objective function that must be minimized is transformed into an optimization issue that must be solved by identifying the Lagrange saddle point and taking derivatives of Lagrange functions $\tilde{J}_m$ with respect to the parameters, i.e., u_{kl} and v_k.

We arrived at this solution by minimizing the objective function (7):

$$u_{kl} = \frac{||\xi_l - v_k||^{-2/(m-1)}}{\sum_{j=1}^{c} ||\xi_l - v_j||^{-2/(m-1)}} \qquad (11)$$

$$v_k = \frac{\sum_{i=1}^{q} \gamma l u_{kl}^{m} \xi_l}{\sum_{i=1}^{q} \gamma l u_{kl}} \qquad (12)$$

According to (11), a matrix $\boldsymbol{U} = [u_{kl}]^{c \times q}$ is obtained. To obtain a stable $\boldsymbol{U}$, (11) and (12) are repeatedly applied until $\max\{\boldsymbol{U}^{(t)} - \boldsymbol{U}^{(t+1)}\} < \eta$, where is the smallest possible error. Due to the fuzzy membership of l to the cluster k, a new membership partition matrix must be constructed. $\boldsymbol{U}' = [u_{kl}]^{c \times N}$ that agrees to the unique image f, is obtained, i.e.,

$$u_{ki} = u_{kl}^{(t)}, if \ x_i = \xi_l \qquad (13)$$

We use membership filtering to improve u ki's membership matrix and speed up our algorithm's convergence. In this research, we use a median filter to balance the performance of membership filtering with the speed of algorithms:

$$U'' = med\{U'\} \qquad (14)$$

The median filtering is med.

The suggested algorithm, M3FCM, can be summarized in the following way.

Step 1: Set the cluster prototype value c, fuzzification parameter
Step 2: Compute the new image ξ using (9), and then compute the
Step 3: Initialize randomly the membership partition matrix $\boldsymbol{U}^{(0)}$.
Step 4: Set the loop counter $t = 0$.
Step 5: Update the clustering centers using (12).
Step 6: Update the membership partition matrix $\boldsymbol{U}^{(t+1)}$ using (11).
Step 7: If $\max\{\boldsymbol{U}^{(t)} - \boldsymbol{U}^{(t+1)}\} < \eta$ then stop, otherwise, set $t = t + 1$ and go to Step 5.
Step 8: Implement median filtering on membership partition mat

3.3.2. Morphological Reconstruction

The pace of convergence of the FCM algorithm is constantly determined by the distribution of data. There is less iteration if the distribution of data favors clustering, while there is more iteration if there are no clusters at all. The distribution properties of data are always impacted by noise corruption, which leads to two issues with FCM because of its sensitivity to noise. Both the segmentation accuracy and iteration time of the FCM algorithm are higher when dealing with noise-corrupted images than when dealing with noise-free images. The histogram is a commonly used tool for analyzing data distribution. Image segmentation is difficult if the histogram is homogeneous. Instead, if the histogram shows numerous distinct peaks, it's simple.

Clustering can be improved by optimizing data distribution before adding MR to FCM algorithm. In order to optimize data distribution characteristics, MR can maintain knowing the noise kind in advance [38].

Morphological dilation and erosion reconstruction are two of the most used MR operations [39]. R f g (g) is the abbreviation for morphological dilation reconstruction.

$$R_f^\delta(g) = \delta_f^{(i)}(g) \qquad (15)$$

where f is the unique image, g is a marker image and $g \leq f, \delta$ signifies dilation process, and $\delta_f^{(1)}(g) = \delta(g) \wedge f, \delta_g^{(i)}(f) = \delta(\delta^{(i-1)}(g)) \wedge f$, and $\wedge$ stands for the point wise minimum.

Reconstruction of morphological erosion is signified by the dual $R_f^\varepsilon(g)$, which is defined as

$$R_f^\varepsilon(g) = \varepsilon_f^{(i)}(g) \qquad (16)$$

where $g \geq f, \xi$ signifies erosion operation, and $\varepsilon_f^{(1)}(g) = \varepsilon(g) \vee f, \varepsilon_g^{(i)}(f) = \varepsilon(\varepsilon^{(i-1)}(g)) \vee f$, and $\vee$ stands for the point wise all-out.

The selection of marker and mask pictures affects the reconstruction result of an image. An image's transformation is considered to be its marker when it is used as a mask for a masking technique. In the real world,, $= \varepsilon(f)$. Thus, $g = \varepsilon(f)$ and $g = \delta(f)$ are continuously used to get a marker image due to easiness and effectiveness.

Operators with greater filtering capabilities, such as morphological opening and closure reconstructions, can be derived from the composition of dilation and erosion reconstructions. As a result of morphological reconstruction, which is referred to by R^C, is more right for texture detail smoothing, we employment R^C to modify unique image. R^C is defined as shadows:

$$R^C(f) = R_{R_f^\delta(\varepsilon(f))}(\delta(R_f^\delta(\varepsilon(f)))) \qquad (17)$$

In [37], the modified image $\xi = (\xi_i)_{i=1}^{N}$ is defined as

$$\xi_i = \frac{1}{1+\alpha}(x_i + \hat{\alpha x}_i) \qquad (18)$$

According to (17), $x_i \in f$ and $\hat{x} \in R^C(f)$, where $R^C(f)$ signifies a reconstructed image obtained by R^C. To get a marker image, an organizing element B counting center element is required for ε or δ, i.e., $\varepsilon_B(f) \leq f$ and $\delta_B(f) \geq f$. Then, R^C is rewritten as

$$R^C(f) = R_{R_f^\varepsilon(\varepsilon_B(f))}^{\varepsilon_\delta}(\delta_B(R_f^\delta(\varepsilon_B(f)))) \qquad (19)$$

For instance, a disk with radius γ can be painstaking as B. If $r = 0$, then $R^C(f) = f$; else f will be smoothed to different degree rendering to the change of r. Therefore, the effect of α is similar to r. And thus, the degree of smoothing will be varied depending on the change in r. As a result, has a comparable impact to r. As a result, we may eliminate the parameter by substituting $R^C(f)$, which eliminates the issue of noise estimation because MR is capable of effectively removing a variety of noise sources.

3.4. Classification

Convolution In situations where the target of local characteristics, the neural network model is an essential feed-forward neural network type. To put it simply, a CNN is made up of a number of convolutional and fully-connected layers. As a result of their strong spatial dependencies in small regions and substantial translation invariance, CNNs are particularly well suited for working with images. Locally connected points in a time series can also be invariant to time shifts.

CNN outperforms existing machine learning algorithms in almost every way possible:-

- (CNN employ adjacent pixel info to effectively down-sample images, and then use a prediction layer at the end to further refine the image's features.
- The convolution operator is used in a variety of ways in CNN.
- Convolutional neural network (CNN) architecture combines the advantages of a regular neural network.

Fully Connected (FC), and Output layers make up a typical deep CNN in this study. Figure 2 shows a basic CNN design.
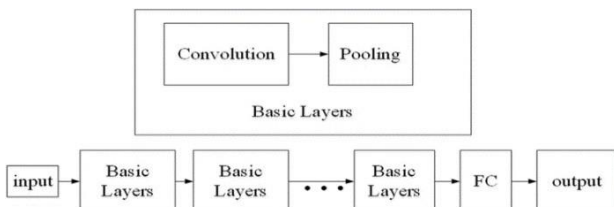

Fig. 2. Basic CNN Architecture

Each part has its own parameters and possessions, convolution layer has:

- The sum of convolution filters (abbreviated as "nb filters")
- A filter's diameter in millimetres (kernel size).
- Strides: The convolution process in a series of steps.
- In order to prevent an issue with convolution, padding is used to add layers of zeros to the input images.
- Activation: This layer is activated by the activation function (Default is linear).
- True bias is employed if this is the case.
- Weights init: the process of starting up the weights.
- The weights can be trained if True.
- Over fitting in machine learning can be alleviated through regularisation. With DropBlock and Shake-Shake, CNN has demonstrated an increase in generalisation performance [40].

There are other limits for pooling, regression and fully connected layer.
For pooling layer:

- Kernel size.
- Padding.
- Strides: Strides of pooling operation.

Fully connected layer has:

- Activation function
- Neurons

Regression Layer:

- In any machine learning model, loss functions play an important role in defining an objective against which the model's performance is judged.
- Faster convergence is made possible by increasing the learning rate. This can have an enormous impact on the output if the learning rate is chosen incorrectly, either too small or too great.
- To minimise the specified loss function, an optimizer is used (which calculate the errors).

Dropout refers to the removal of units from a neural network, both apparent and hidden. Keep Probability is a concept. For example, a forward or backward pass is made by "ignoring" these units [41].

3.4.1. Network Training

An example (picture) is propagated across a network and its weights (signed random values) are modified by iteratively modifying the weights. Batches are used to break up the presentation of all training instances into smaller units, which are called epochs (256 image patches in our approach). When a batch is finished, the weight of each unit is updated based on the back propagated errors it has committed. The error Backpropagation algorithm enhanced with dropout [42] is one of the training methods offered by DL. Even though the algorithm can be found in every NN textbook, dropout is a more recent development and is hence the subject of the following description. Dropouts randomly select and temporarily' switch off' a subset of network units (usually 50%) during training. When an example is shown, these units do not propagate signals (their outputs are constrained to zero) nor do they participate in the error Backpropagation process.

4. Results and Discussions

4.1. Segmentation Analysis

F1 score, Accuracy, Sensitivity, and Specificity are some of the measures we utilize to measure performance. The best model is one that has all of these markers at 1. The following are the formulas for calculating various metrics:

$$Accuracy = (TP+TN)/(TP+TN+FP+FN') \tag{20}$$

$$Sensitivity = TP/(TP+FN') \tag{21}$$

$$Specificity = TN/(TN+FP') \tag{22}$$

$$F1 = 2 \times (Precision \times Recall)/(Precision+Recall) \tag{23}$$

Where TP denotes the correctly identified pixel. TN is the pixel in the background that has been accurately identified. FP is the mislabeled background pixel. FN is a wheat picture pixel that has been incorrectly labeled. The proposed segmentation model's graphical results are shown in Figure 3.

Fig. 3. Graphical Results of Proposed Segmentation

Table 1: Segmentation Results of Various FCM model with Proposed System

Model Name	Sensitivity	Specificity	F1	Accuracy	AUC
Basic FCM	0.8196	0.9748	0.8286	0.9703	0.9870
Multi-output fusion FCM	0.8192	0.9810	0.8293	0.9705	0.9870
Multi-scale FCM	0.8115	0.9760	0.8290	0.9707	0.9873
Multi-path FCM	0.8118	0.9808	0.8287	0.9706	0.9871
Proposed system	0.8325	0.9838	**0.8321**	0.9806	**0.9880**

In figure 4 and table 3 represent that the results of various fcm model with proposed System, in this comparison analysis Basic FCM reached the accuracy of 0.9703% respectively. Another, the Multi-output fusion FCM model reached the accuracy of 0.9705%, which is little same for basic FCM technique. And the Multi-scale FCM attained the accuracy of 0.9873=8%, which reached little bit higher than other two methods. Multi-path FCM attained the accuracy of 0.9871, which lower than Multi-path FCM. Finally the proposed model the accuracy of 0.9880%, which is top most accuracy than all compared methods.
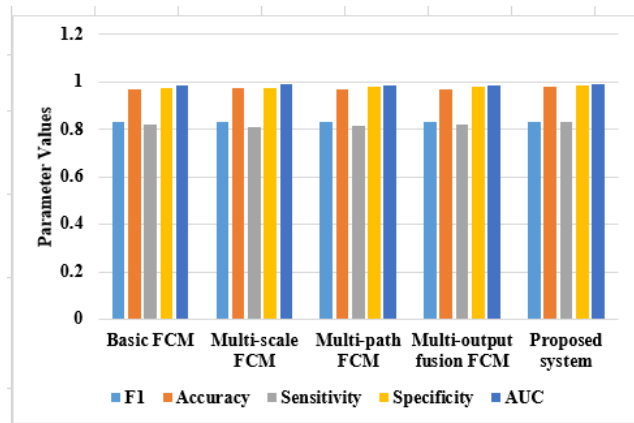

Fig. 4. Graphical Representation of Proposed Segmentation model

4.2. Classification Results

Sensitivity, specificity, accuracy, and false measure are all considered when making a classification. The following are the criteria for measuring success:

$$\text{Accuracy} = (tp+tn)/N \qquad (24)$$

$$\text{sensitivity} = tp\_rate \qquad (25)$$

$$\text{specificity} = tn\_rate \qquad (26)$$

$$\text{precision} = tp/ (tp+fp) \qquad (27)$$

$$\text{recall} = tp/ (tp+fn) \qquad (28)$$

$$\text{f\_measure} = 2*((\text{precision}*\text{recall})/ (\text{precision} + \text{recall})) \qquad (29)$$

$$\text{gmean} = sqrt(tp\_rate*tn\_rate) \qquad (30)$$

Where tp,tn,fp and fn denote the number of a true positive, true negative, false positive and false negative, N describes the total sum of elements. Table 2 and 3 shows the classification results of proposed model with existing techniques.

Table 2: Comparative Analysis of projected ideal with existing classifiers

Classification Technique	Sensitivity	Specificity	Precision	Recall	G-mean
Auto-encoder	0.9715	0.8958	0.0884	1.0000	0.9465
LSTM	0.9814	0.9085	0.0994	1.0000	0.9531
RNN	0.9988	0.9258	0.1699	1.0000	0.9622
CNN	**0.9999**	**0.9500**	**0.1841**	**1.0000**	**0.9795**

Fig. 5. Graphical Comparison of Proposed Classifier

Comparative Analysis of proposed model with existing classifiers is showed in table 2 and figure 5. Here we used different
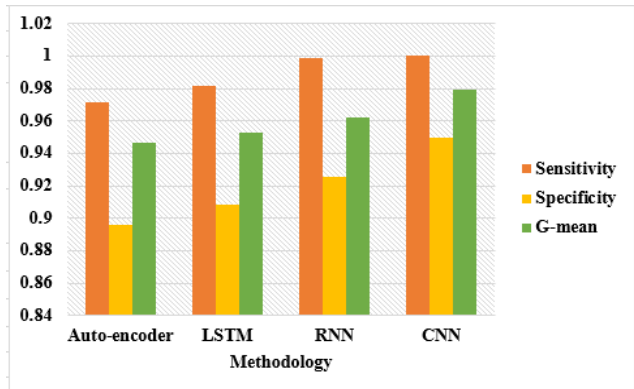
classifiers as Auto-encoder, LSTM, RNN and CNN. In this comparison analysis, the auto-encoder reached the G-mean of 0.9465%. Another classifier model of LSTM reached the G-mean of 9531%. Finally, the CNN classifier model reaches the G-mean of 9795% respectively. By seeing this comparison analysis, the proposed model reached the highest G-mean.

Table 3: Experimental Analysis of proposed model with existing classifiers

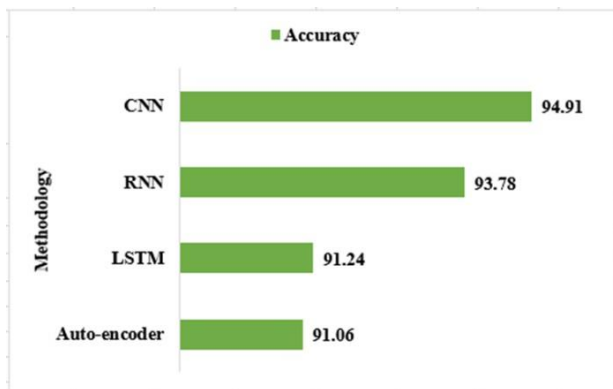| Classification Technique	Accuracy	F-measure
Auto-encoder	91.06	0.1724
LSTM	91.24	0.1908
RNN	93.78	0.2240
CNN	**94.91**	**0.2720**

Fig. 6. Graphical Comparison of Proposed Classifier in terms of Accuracy

In figure 6 and table 3 represent that the experimental analysis of proposed model with existing classifiers. The classification techniques as Auto-encoder, LSTM, RNN and CNN, in this comparisons analysis the Auto-encoder reached the accuracy of 91.06 and the F-measure value of 0.1724. LSTM classifier model attained the accuracy of 91.24 and F-measure of 0.1908. And another RNN reached the accuracy of 93.78% and the F-measure of 0.2240%CNN accuracy of 94.91% F-measure of 0.2720% respectively. By seeing this comparison analysis, the proposed model reached the highest accuracy and F-measure respectively.

5. Conclusion

In order to enhance segmentation excellence and limit the impact of picture noise, a significantly fast and robust M3FCM algorithm for segmentation is proposed in this study. The local spatial info of pictures has been used to enhance the segmentation effect of MR operations. A compromise between noise reduction and preservation of fine details has been made possible because to MR's ability to suppress noise while maintaining an object's shape. In addition, MR is able to rebuild images that have been distorted by a variety of various types of noise. M3FCM also used membership filtering to take use of the local geographical constraint in the dataset. When compared to local spatial limitation, we found that membership filtering can get identical results; however membership filtering takes substantially longer per iteration. The suggested M3FCM has been shown to produce improved segmentation results without the need to tune parameters for different wheat images in experiments. For the final disease prediction, the segmented leaves are fed into a CNN. CNN achieved 99.9% sensitivity and 95.5% specificity, whereas the suggested model has 98% sensitivity and 98% AUC, which is better than existing models.\

References

[1] Curtis, B.C.; Rajaram, S.; Gomez Macpherson, H. Bread Wheat: Improvement and Production; Food and Agriculture Organization of the United Nations (FAO): Rome, Italy, 2002.

[2] Figueroa, M.; Hammond-Kosack, K.E.; Solomon, P.S. A review of wheat diseases—A field perspective. Mol. Plant Pathol. 2018, 19, 1523–1536.

[3] Shamanin, V.; Pototskaya, I.; Shepelev, S.; Pozherukova, V.; Salina, E.; Skolotneva, E.; Hodson, D.; Hovmøller, M.; Patpour, M.; Morgounov, A. Stem rust in Western Siberia—Race composition and effective resistance genes. Vavilov J. Genet. Breed. 2020, 24, 131–138.

[4] Sanin, S.S. Epiphytotics of Cereal Crops Diseases: Theory and Practice. Izbrannye Trudy; Voshod-A: Moscow, Russia, 2012; pp. 161–166. (In Russian)

[5] Bhathal, J.S.; Loughman, R.; Speijers, J. Yield reduction in wheat in relation to leaf disease from yellow (tan) spot and septoria nodorum blotch. Eur. J. Plant Pathol. 2003, 109, 435–443.

[6] Ficke, A.; Cowger, C.; Bergstrom, G.; Brodal, G. Understanding yield loss and pathogen biology to improve disease management: Septoria nodorum blotch—A case study in wheat. Plant Dis. 2018, 102, 696–707.

[7] Simón, M.R.; Ayala, F.M.; Golik, S.I.; Terrile, I.I.; Cordo, C.A.; Perelló, A.E.; Moreno, V.; Chidichimo, H.O. Integrated foliar disease management to prevent yield loss in Argentinian wheat production. Agron. J. 2011, 103, 1441–1451.

[8] Broers, L.H.M. Influence of development stage and host genotype on three components of partial resistance to leaf rust in spring wheat. Euphytica 1989, 44, 187–195.

[9] Parker, S.R.; Shaw, M.W.; Poyle, D.J. The reliability of visual estimates of disease severity on cereal leaves. Plant Pathol. 1995, 44, 856–864.

[10] Bock, C.H.; Poole, G.H.; Parker, P.E.; Gottwald, T.R. Plant disease severity estimated visually, by digital photography and image analysis, and by hyperspectral imaging. Crit. Rev. Plant Sci. 2010, 29, 59–107.

[11] Martinelli, F.; Scalenghe, R.; Davino, S.; Panno, S.; Scuderi, G.; Ruisi, P.; Villa, P.; Stroppiana, D.; Boschetti, M.; Goulart, L.R.; et al. Advanced methods of plant disease detection. A review. Agron. Sustain. Dev. 2015, 35, 1–25.

[12] Farber, C.; Mahnke, M.; Sanchez, L.; Kurouski, D. Advanced spectroscopic techniques for plant disease diagnostics. A review. Trends Anal. Chem. 2019, 118, 43–49.

[13] Mahlein, A.K. Plant disease detection by imaging sensors-parallels and specific demands for precision agriculture and plant phenotyping. Plant Dis. 2016, 100, 241–251.

[14] Lindow, S.E.; Webb, R.R. Quantification of foliar plant disease symptoms by microcomputer-digitized video image analysis. Phytopathology 1983, 73, 520–524.

[15] Camargo, A.; Smith, J.S. An image-processing based algorithm to automatically identify plant disease visual symptoms. Biosyst. Eng. 2009, 102, 9–21.

[16] Dammer, K.H.; Möller, B.; Rodemann, B.; Heppner, D. Detection of head blight (Fusarium ssp.) in winter wheat by color and multispectral image analyses. Crop Prot. 2011, 30, 420–428.

[17] Ma, J.; Du, K.; Zhang, L.; Zheng, F.; Chu, J.; Sun, Z. A segmentation method for greenhouse vegetable foliar disease spots images using color information and region growing. Comput. Electron. Agric. 2017, 142, 110–117.

[18] Bebronne, R.; Carlier, A.; Meurs, R.; Leemans, V.; Vermeulen, P.; Dumont, B.; Mercatoris, B. In-field proximal sensing of septoria tritici blotch, stripe rust and brown rust in winter wheat by means of reflectance and textural features from multispectral imagery. Biosyst. Eng. 2020, 197, 257–269.

[19] Singh, A.K.; Ganapathysubramanian, B.; Sarkar, S.; Singh, A. Deep learning for plant stress phenotyping: Trends and future perspectives. Trends Plant Sci. 2018, 23, 883–898.

[20] Alzubaidi, L.; Zhang, J.; Humaidi, A.J.; Al-Dujaili, A.; Duan, Y.; Al-Shamma, O.; Santamaría, J.; Fadhel, M.A.; Al-Amidie, M.; Farhan, L. Review of deep learning: Concepts, CNN architectures, challenges, applications, future directions. J. Big Data 2021, 8, 1–74.

[21] Krizhevsky, A.; Sutskever, I.; Hinton, G.E. Imagenet

classification with deep convolutional neural networks. Adv. Neur. Inf. Proc. Syst. 2012, 25, 1097–1105.

[22] Simonyan, K.; Zisserman, A. Very deep convolutional networks for large-scale image recognition. arXiv 2014, arXiv:1409.1556.

[23] He, K.; Zhang, X.; Ren, S.; Sun, J. Deep Residual Learning for Image Recognition. In Proceedings of the IEEE Conference on Computer Vision and Pattern Recognition (CVPR), Las Vegas, NV, USA, 26 June–1 July 2016; pp. 770–778.

[24] Howard, A.G.; Zhu, M.; Chen, B.; Kalenichenko, D.; Wang, W.; Weyand, T.; Weyand, T.; Andreetto, M.; Adam, H. Mobilenets: Efficient convolutional neural networks for mobile vision applications. arXiv 2017, arXiv:1704.04861.

[25] Hu, J.; Shen, L.; Sun, G. Squeeze-and-excitation networks. In Proceedings of the IEEE Conference on Computer Vision and Pattern Recognition (CVPR), Salt Lake City, UT, USA, 18–22 June 2018; pp. 7132–7141.

[26] Toda, Y.; Okura, F. How convolutional neural networks diagnose plant disease. Plant Phenomics 2019, 2019, 9237136.

[27] Saleem, M.H.; Potgieter, J.; Arif, K.M. Plant disease detection and classification by deep learning. Plants 2019, 8, 468.

[28] Hasan, R.I.; Yusuf, S.M.; Alzubaidi, L. Review of the state of the art of deep learning for plant diseases: A broad analysis and discussion. Plants 2020, 9, 1302.

[29] Duong, L.T.; Nguyen, P.T.; Di Sipio, C.; Di Ruscio, D. Automated fruit recognition using EfficientNet and MixNet. Comp. Electron. Agric. 2020, 171, 105326.

[30] Gao, Z.; Luo, Z.; Zhang, W.; Lv, Z.; Xu, Y. Deep learning application in plant stress imaging: A review. AgriEngineering 2020, 2, 430–446.

[31] Goyal, L., Sharma, C.M., Singh, A. and Singh, P.K., 2021. Leaf and spike wheat disease detection & classification using an improved deep convolutional architecture. Informatics in Medicine Unlocked, 25, p.100642.

[32] Khan, I.H., Liu, H., Li, W., Cao, A., Wang, X., Liu, H., Cheng, T., Tian, Y., Zhu, Y., Cao, W. and Yao, X., 2021. Early Detection of Powdery Mildew Disease and Accurate Quantification of Its Severity Using Hyperspectral Images in Wheat. Remote Sensing, 13(18), p.3612.

[33] Wójtowicz, A., Piekarczyk, J., Czernecki, B. and Ratajkiewicz, H., 2021. A random forest model for the classification of wheat and rye leaf rust symptoms based on pure spectra at leaf scale. Journal of Photochemistry and Photobiology B: Biology, 223, p.112278.

[34] Schirrmann, M., Landwehr, N., Giebel, A., Garz, A. and Dammer, K.H., 2021. Early detection of stripe rust in winter wheat using deep residual neural networks. Frontiers in Plant Science, 12, p.475.

[35] Hayit, T., Erbay, H., Varçın, F., Hayit, F. and Akci, N., 2021. Determination of the severity level of yellow rust disease in wheat by using convolutional neural networks. Journal of Plant Pathology, 103(3), pp.923-934.

[36] Genaev, M.A., Skolotneva, E.S., Gultyaeva, E.I., Orlova, E.A., Bechtold, N.P. and Afonnikov, D.A., 2021. Image-based wheat fungi diseases identification by deep learning. Plants, 10(8), p.1500.

[37] L. Szilagyi, Z. Benyo, S. M. Szilagyii, and H. S. Adam, "MR brain image segmentation using an enhanced fuzzy c-means algorithm," in Proc. 25th Annu. Int. Conf. IEEE Eng. Med. Biol. Soc., 2003, pp. 17–21.

[38] A. M. Mendonca and A. Campilho, "Segmentation of retinal blood vessels by combining the detection of centerlines and morphological reconstruction," IEEE Trans. Med. Imag., vol. 25, no. 9, pp. 1200–1213, Sep. 2006.

[39] J. J. Chen, C. R. Su, W. E. L. Grimson, J. L. Liu, and D. H. Shiue, "Object segmentation of database images by dual multiscale morphological reconstructions and retrieval applications," IEEE Trans. Image Process., vol. 21, no. 2, pp. 828–843, Feb. 2012

[40] Wang Y, Bian Z-P, Hou J, Chau L-P. Convolutional neural networks with dynamic regularization. 2019; arXiv preprint arXiv:1909.11862

[41] Gal Y, Ghahramani Z. Dropout as a bayesian approximation: Representing model uncertainty in deep learning. In: International Conference on Machine Learning, 2016:1050–1059

[42] N. Srivastava, G. Hinton, A. Krizhevsky, I. Sutskever, and R. Salakhutdinov, "Dropout: A simple way to prevent neural networks from overfitting," J. Mach. Learn. Res., vol. 15, no. 1, pp. 1929–1958, 2014.Boston, MA, USA, 1985, pp. 585–590.